CrossMark

ORIGINAL ARTICLE

The multi-modal responses of a physical head model subjected to various blast exposure conditions

S. Ouellet[1] · M. Philippens[2]

Abstract The local and global biomechanical response of the body to a blast wave is the first step of a sequence that leads to the development of stresses and strains which can exceed the tolerance of brain tissue. These stresses and strains may then lead to neuro-physical changes in the brain and contribute to initiate a cascade of events leading to injury. The specific biomechanical pathways by which the blast energy is transmitted through the head structure are, however, not clearly understood. Multiple transmission mechanisms have been proposed to explain the generation of brain stresses following the impingement of a blast wave on the head. With the use of a physical head model, the work presented here aims at demonstrating that the proposed transmission mechanisms are not mutually exclusive. They are part of a continuum of head responses where, depending on the exposure conditions, a given mechanism may or may not dominate. This article presents the joint analysis of previous blast test results generated with the brain injury protection evaluation device (BIPED) headform under four significantly different exposure conditions. The focus of the analysis is to demonstrate how the nature of the recorded response is highly dependent on the exposure characteristics and consequently, on the method used to reproduce blast exposure in a laboratory environment. The timing and magnitude of the variations in intra-cranial pressures (ICP) were analysed relative to the external pressure field in order to better understand the wave dynamics occurring within the brain structure of the headform. ICP waveforms were also analysed in terms of their energy spectral density to better identify the energy partitioning between the different modes of response. It is shown that the BIPED response is multi-modal and that the energy partitioning between its different modes of response is greatly influenced by exposure characteristics such as external peak overpressure, impulse, blast wave structure, and direction of propagation. Convincing evidence of stresses generated from local skull deformation is presented along with evidence of stress transmission through relative brain-to-skull motion. These findings suggest that research aimed at defining exposure thresholds should not focus on a single stress transmission mechanism or use experimental designs unrepresentative of realistic blast loading conditions that may favour a given mechanism over another.

1 Introduction

In the general sense, the *injury mechanisms* of blast neuro-trauma (BNT) are used to describe the sequence of biomechanical and pathophysiological responses that follow exposure to a blast wave, and that ultimately lead to acute and/or chronic neurological dysfunction. It is the local and global biomechanical response of the body to this mechanical insult that leads to the development of stresses and strains that exceed the tolerance of brain tissue. Brain stresses and strains may lead to neuro-physical changes and contribute to initiating an injury cascade. Unfortunately, the specific

The second author name was published with incorrect spelling. It should read as M. Philippens. Now, it has been corrected.

✉ S. Ouellet
simon.ouellet@drdc-rddc.gc.ca

1 Defence Research and Development Canada, 2459 de la Bravoure rd, Quebec, QC G3J 1X5, Canada

2 TNO Rijswijk, Lange Kleiweg 137, 2288 GJ Rijswijk, The Netherlands

🍂 Springer

biomechanical pathways, or energy transmission mechanism, by which the blast energy is transmitted through the head structure to generate these injurious stress states are not well understood [1–4]. In addition, the sensitivity of brain tissue to dynamic loading conditions remains unclear [5,6].

1.1 Biomechanical pathways

Several types of biomechanical pathways have been proposed. Although there are variations that arise in the interpretation of the proposed pathways, they can typically be grouped in three or four categories. We choose to distinguish between four categories, as illustrated in Fig. 1:

1. Direct cranial entry or trans-osteal wave propagation.
2. Generation of stress waves in the brain due to the rapid structural deformation of the skull (skull flexure or bending).
3. Generation of stresses into the brain due to head acceleration and relative brain-to-skull motion.
4. Transmission of stresses into the brain through vascular pressure surge due to rapid thoracic compression.

While some authors have not differentiated between the first two transmission mechanisms [1,2], simply labelling them as direct transmission, other authors have deemed it necessary to distinguish between instantaneous wave transmission through material interfaces and the generation of stress waves from the skull structural deformation [7–10].

Direct cranial entry refers to the successive transmission of stresses through the interface of neighbouring materials of different impedances (air to skin, skin to skull, etc.). It may also include direct entry via the various foramina [3]. Assuming that the peak incident overpressures (OPs) of interest for the study of blast-induced neuro-trauma are typically under 1 MPa [11], it is reasonable to assume that the stress waves transmitted directly into the skin and underlying skull are elastic in nature, travelling at acoustic speeds. This partly explains why authors have suggested using simple acoustic transmission models to estimate the level of generated stress, in a given structure, upon loading from a blast wave [12]. However, it has been shown that these models alone fail to predict the transmission of stresses from a blast wave through multiple thin interfaces [12,13]. More sophisticated models accounting for layer thicknesses have been developed to help in the design of thoracic blast protection systems [14]. Such models, when applied to the head structure, would suggest that the impedance mismatch offered by the skull may limit transmission of the blast energy to a narrow band of the blast wave spectrum. Bolander et al. [7] also suggested that direct cranial entry alone may only result in very low-magnitude, high-frequency perturbations in the brain. It appears that this pathway alone cannot explain the level of brain stresses observed experimentally after exposure to a blast wave.

On the other hand, skull flexure has been shown to generate significant intra-cranial pressure following blast exposure [7–10,15]. This pathway refers to the structural deformation of the skull structure in response to the high-rate loading from the blast. As the blast wave reflects from and diffracts around the head, a transient pressure field develops around the head and causes a structural response before any significant global motion of the head occurs. This structural response includes the initial local deformation of the skull where the blast wave reflection is maximal, but also any natural modal response (or bending modes) of the skull that occurs as a result of stress waves propagating back and forth in the structure. This rapid deformation of the skull will in turn induce stress waves in the brain, which may be compressive, tensile, or shear waves [3]. High local stresses in the brain may also arise from constructive interference between waves which had entered the brain from distinct locations. This pathway may also lead to cerebrospinal fluid (CSF) or brain tissue cavitation arising from excessive tensile stress states.

Traumatic brain injury (TBI) induced from head acceleration or low velocity impact has been the topic of considerable research [16–18], mainly in the fields of automotive crash safety and sports injury prevention. As such, it appears natural to propose that accelerations induced by the exposure to a blast wave could be a biomechanical pathway leading to BNT. In the context of blast, this pathway refers to global,
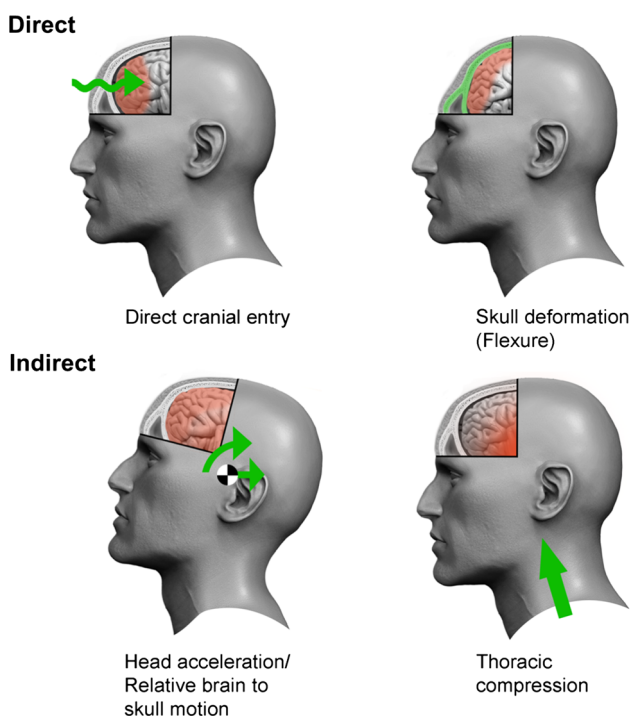

Direct

Direct cranial entry

Skull deformation (Flexure)

Indirect

Head acceleration/ Relative brain to skull motion

Thoracic compression

Fig. 1 Proposed biomechanical pathways for the transmission of the blast wave energy to the brain

macroscopic head motion which can generate brain stresses indirectly through inertial forces or through a decoupling of the brain motion relative to the skull (Fig. 1). Relative brain-to-skull motion may lead to the shearing of bridge veins at the interface. It can cause localized brain contusion at the *coup site*, the region of the brain facing the blast source, where the skull may move into the brain and locally create excessive contact forces. The decoupled motion of the skull relative to the brain can also create tensile stresses at the opposite side of the head, the *contre-coup* site, where the skull may locally and rapidly move away from the brain. Blast-induced head accelerations can be translational and rotational, the proportions of which may be specific to the blast loading orientations. It has been highlighted that even purely translational head acceleration may, however, induce both linear and angular displacement of the brain relative to the skull due to the asymmetry of the brain and attachment to the brain stem [3].

The fourth proposed pathway refers to stresses originating from the thorax and reaching the brain structure, through a vascular pressure surge following rapid compression of the chest or stress wave transmission through the vasculature and soft tissues. There is increasing evidence for the contribution of this mechanism to the development of blast neuro-trauma [19–22]. However, due to the nature of the experimental work presented in this paper, which considers the use of a head-form for studying the biomechanical pathways by which the blast energy reaches the brain, we will not elaborate further on this mechanism.

There is contradictory evidence for and against the afore-mentioned three mechanisms, as reviewed recently by Court-ney et al. [1]. This may be largely due to the wide variety of experimental designs and exposure conditions used in BNT studies. Needham et al. noted: "an increase in the number of blast injury studies that have utilized improperly conceived experiments", and that "confusion has been compounded by a misunderstanding of the differences between the loading produced by a free-field explosive blast and that produced by a conventional shock tube" [23]. Matching peak static over-pressure does not guarantee that the full blast wave profile is relevant to real-life scenarios [24]. The blast wave positive phase duration and total positive impulse are critical loading parameters that need to be reproduced closely. Also, shock tube experiments using high blockage ratio or the jet emerging from the end of the tube are particularly prone to creating unrealistic loading conditions [25]. At the source of confusion is the contribution of the dynamic component of pressure to the full OP field history experienced by a target. The blast flow field in an end jet or in an obstructed shock tube differs significantly from that in an open field. While experiments may adequately reproduce the static OP history from a free-field blast, errors of orders of magnitude may occur in the dynamic component of the loading [23,25]. Such dif-

ferences could favour one biomechanical pathway over the other. For example, global head motion may be significantly enhanced by a dramatic increase in dynamic OP.

Researchers have acknowledged the non-exclusive nature of the proposed biomechanical pathways [1–3]. Neverthe-less, individual pathways were studied in isolation or in a decoupled fashion [26,27]. It was observed that significantly different loading conditions that encouraged one pathway over another resulted in different pathophysiology [26]. A study using an advanced blast simulator (ABS) and an animal model compared two loading conditions: one with the head immobilized and the other one with the head unconstrained. The study reported a marked difference in the nature of the injury outcome [27]. This finding could suggest that since the separate biomechanical pathways induced, in isolation, different injury phenotype, they are probably uncoupled. In other words, they likely generate spatially separated stress states into the brain. However, this does not guarantee that brain stresses generated from different pathways cannot interact under certain loading conditions to develop transient stress states in the same regions of the brain.

Willinger and colleagues approached the modelling of head responses for TBI studies using modal analysis [28]. They treated skull flexure and brain-to-skull relative motion as part of the same time/frequency continuum, where each pathway has a range of timescales or frequencies associ-ated with it. They identified the relevant timescales and showed through mathematical modelling that different types of responses had specific natural frequencies. They proposed that each response mode is excited by different loading char-acteristics. They argued that the duration of the applied loading dictates the nature of the strain and stress field in the brain and therefore the type of observed lesions. They established that for long loading durations (10–12 ms), the head is globally subjected to the same translational and rota-tional acceleration field and that inertial forces dominate, leading to distributed lesions throughout the brain volume. For medium loading durations (4–10 ms), the motion of the skull and the brain become decoupled and the relative displacements lead to bridge vein shearing and focused con-tusions in the case of excessive skull–brain contact forces. For this type of response in particular, they identified a nat-ural frequency for the head between 100–150 Hz. For short loading durations below 4 ms, the load is delivered rapidly enough that the skull does not have time to reach force equi-librium. The skull does not move as a rigid body anymore but deforms locally and generates compressive, tensile, and shear intra-cranial stresses in nearby brain regions. They identi-fied a second natural frequency, associated with this type of response, between 700 and 800 Hz. The simple model pro-posed by Willinger et al. identified natural frequencies that are in agreement with previously published work focusing on individual response modes [29–31]. They also obtained good

correlation with accident reconstruction data where different individual modes were excited [32].

The model proposed by Willinger et al. did not account for all characteristics of a loading scenario (e.g. rise time and decay profile). Nevertheless, the modal analysis presented by Willinger is very relevant to the discussion on blast neuro-trauma injury mechanisms. A single blast wave with specific static and dynamic OP histories can load the head structure on different timescales. The initial rise in OP may be a very high frequency phenomenon, while the full history of the blast OP may be composed of lower-frequency fluctuations. The assumption behind the work reported herein is that blast waves can trigger all different modes of response and reach the brain through various pathways within a single event. Depending on the characteristics of the blast wave, some pathways may dominate the generation of brain stresses or all mechanisms may overlap each other and contribute relatively equally to the stress history.

1.2 Head surrogates

Instrumented physical models of the human head, also called headforms or head surrogates, have been used to study the biomechanical response of the human head under dynamic loading for decades. Solid and relatively homogeneous head models such as the Hybrid III headform are used in conjunction with injury risk functions to assess the effects from indirect accelerative loadings. Unfortunately, such simplified headforms are developed on the basis that the global head acceleration history alone can be correlated to the risk of sustaining a certain level of injury.

Capturing the more direct biomechanical pathways requires a larger set of biofidelic features to ensure that the local and modal response of the head structure is representative. These features include anthropomorphic external and internal components as well as a material selection that can imitate human tissue response under the range of relevant loading rates.

Recently, headforms optimized for blast loading conditions have been developed [33–36]. Such headforms are typically composed of skin, skull, and brain simulants and mounted on a flexible neck assembly. They are typically instrumented with both external and intra-cranial sensors. They allow for the observation of pathways which cannot be observed with simpler homogeneous models. However, the observation of a dominant energy transmission mechanism can be influenced by headform design choices. For example, it was observed from tests with the realistic explosive dummy (RED) headform that biomechanical loading of the brain is governed by direct wave transmission, structural deformations, and wave reflections from tissue–material interfaces [35]. While this is very relevant, the physical model used in this study did not allow for brain-to-skull relative motion
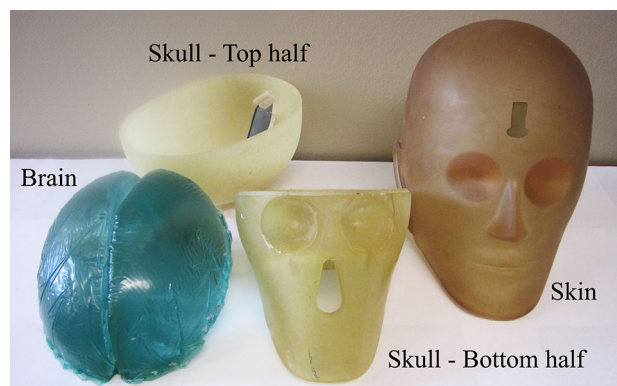

Fig. 2 BIPED skull, brain, membrane, and skin surrogates, not including any instrumentation

as the brain medium completely filled the cranial cavity. The dominant character of direct transmission pathways may therefore be artificial, as other non-direct transmission mechanisms may be mitigated. An alternative design choice was made for the John Hopkins University Applied Physics Laboratory headform [36,37]. The brain of the headform is coated with a silicone oil prior to being installed in the cranium in order to provide a slip boundary condition at the skull interface. However, the brain fills the cranial cavity and no CSF simulant was used.

The BIPED headform (Fig. 2) is an instrumented physical model of the head with general anthropomorphic features and the necessary anatomical structures that allows for the capture of both global and local response of the head under blast loading. Developed at Defence Research and Development Canada (DRDC)—Valcartier Research Center, the BIPED is composed of a skin, skull, brain, cerebellum, CSF, falx membrane, and tentorium membrane simulants. The simulants are made of materials that were selected to represent the elastic or visco-elastic response of their biological counterparts. The headform is mounted on a 50th percentile HIII neck assembly [38]. It is capable of monitoring head external pressure field history at five locations (forehead, right side, left side, top, and back) as well as intra-cranial pressures at four locations (frontal, temporal, parietal region) and global translational and rotational accelerations. The model allows for brain-to-skull relative motion. However, the brain boundary conditions remain to be validated. The brain simulant is currently suspended in CSF and restrained by the falx and tentorium membrane, but it is not attached to a structure mimicking the spinal cord. The BIPED demonstrated excellent reproducibility both between test repeats and between different copies of the headform [33,34].

Through the detailed replication of blast tube experiments that were previously reported [39], the intra-cranial response of the BIPED was compared to that of post-mortem human specimens (PMHS) [34]. Laboratory setup, loading condi-
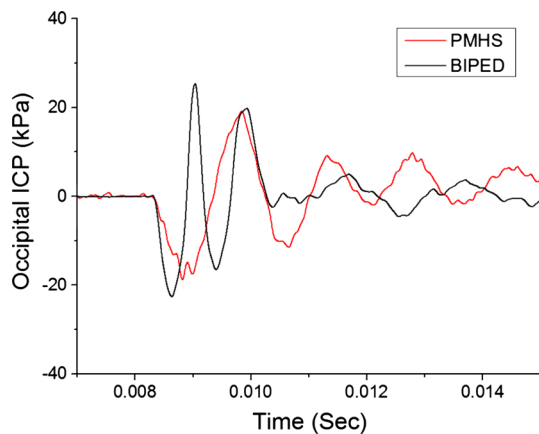
Fig. 3 Comparison of the BIPED and PMHS occipital ICP response for a generated blast with a peak static overpressure of 70 kPa

tions, instrumentation, and head mounting technique were reproduced identically. A direct comparison of measured early-time ICP was obtained for three blast intensities (80, 100, and 120 kPa), two exposure orientations (parallel and perpendicular), and at three brain locations (frontal, occipital, and parietal). The level of agreement was evaluated in terms of peak ICP and Fourier spectrum. The ICP magnitudes were found to be within 15% of the PMHS values, while the headform appeared to have a natural mode of response at a slightly higher frequency than the PMHS. In general, the damping of the ICP signals also appeared to be greater for the BIPED. The test favoured the structural response of the head over the global motion response because the PMHS and the BIPED were rigidly suspended in the blast tube. The tests were considered a validation of the direct biomechanical pathways of the BIPED, as opposed to the full response. Figure 3 shows one representative example of the comparison of a BIPED ICP signal with a PMHS ICP signal at the occipital location for the low-level exposure.

1.3 Current study

The work presented herein aims to further demonstrate, by using the BIPED headform, that the different proposed biomechanical pathways are not mutually exclusive but rather part of a continuous function. Depending on the exposure conditions, a given mechanism may or may not dominate the brain response. Furthermore, the work aims at demonstrating that identifying in isolation the independent injury thresholds for the different possible injury mechanisms may not be appropriate. The different mechanisms contribute to developing stresses in similar regions of the brain and on a similar timescale.

This article presents the joint analyses of blast test results generated with the BIPED under various conditions of exposure obtained through the use of different methods to generate

a blast wave. Four sets of conditions are analysed and compared to highlight the correlation between exposure conditions and contributing biomechanical pathways. In particular, we investigate the response of the headform to:

A. A spherical free-field blast from the above-ground detonation of a bare explosive charge.
B. A hemispherical free-field blast from the near-ground detonation of a bare explosive charge.
C. A blast obtained from an explosively driven rectangular shock tube.
D. A blast obtained from a breaching exercise.

These test conditions were chosen to provide a wide range of exposure characteristics. In particular, the intention was to analyse blast conditions that had low, normal, and enhanced dynamic OP components. Not all of the generated blasts were meant to reproduce loading characteristics that are relevant to military operation. The focus of the analyses was to demonstrate how the recorded ICP response is highly dependent on the exposure characteristics and consequently on the method used to reproduce the exposure in the laboratory. The timing and magnitude of the BIPED ICP fluctuations were analysed relative to the recorded external transient pressure field in order to better understand the stress wave dynamics occurring within the brain structure. ICP waveforms were also analysed in terms of their energy spectral density to observe the energy partitioning between the different modes of response and the contribution from particular biomechanical pathways.

2 Method

2.1 BIPED headform

Relevant information on the BIPED construction, material selection, and instrumentation is given below. Extensive details are provided in [33,34].

The headform weighs approximately 3.8 kg, which is found to be within the standard deviation for the average human head mass, where for head dimensions between the 25–75th percentile, an average head weight of 4.1 ± 0.6 kg was obtained in previous research [40]. The BIPED skull is moulded in two parts to allow insertion of the brain. The joint is on a horizontal plane above the eye orbital cavity. After sealing, the cranial cavity is filled with a saline water mixture, simulating the CSF, and only a small volume of air is left at the top of the skull to prevent the development of excessive ICP. The CSF simulant ensures that the brain is neutrally buoyant. It is uniformly dispersed around the brain. The position of the brain within the cavity is verified via X-ray imaging after assembly (Fig. 4). It is assumed that any
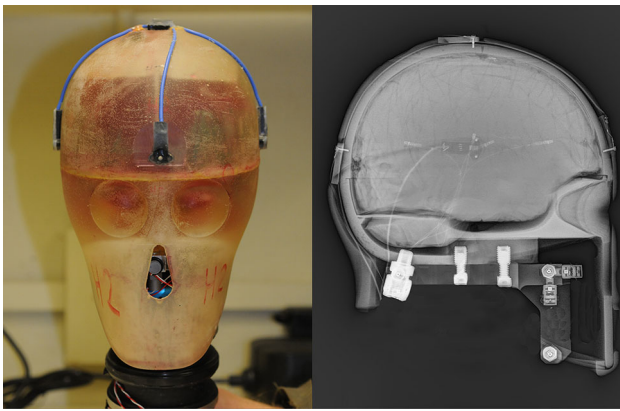
Fig. 4 **a** External pressure transducers and **b** ICP transducer positioning

gap between the brain and the skull on the X-ray images is filled with the CSF simulant. The BIPED skin and skull have a uniform thickness of 6.35 and 6.9 mm, respectively. The skin is tightly fit on the skull.

The brain is only constrained and kept in position by the falx and tentorium membranes, which are both 1.5 mm in thickness and run between the two brain hemispheres and between the cerebellum and occipital lobe, respectively. The brain surface is smooth, and its geometry follows the geometry of the inner surface of the skull with a recess of approximately 2 mm.

The headform is mounted on a 50th percentile Hybrid III neck. It is recognized that the HIII neck has greater neck flexural stiffness than the human neck and does not allow for any initial translational motion of the head. This is a physical limitation to the model which may underrepresent the magnitude of the contribution of head global motion. Also, the HIII neck has less damping than the human neck, which may cause the head to artificially rebound from back to front following the exposure to a blast.

In the BIPED, the selection of surrogate materials was focused on matching the small strain elastic response and the density of the biological materials, therefore also matching elastic wave speeds. Another requirement for the headform was to be reusable and highly reproducible; thus, permanent deformation of any component had to be avoided within the expected range of operation. Materials also had to offer good robustness and easy manufacturability.

The skull in particular is made of a single isotropic casting polymer. Based on experimental measurements of the compressive elastic modulus and density of the polymer used for the skull, longitudinal wave speed was estimated around 2000 m/s. The longitudinal wave speed for the skull bone assembly was estimated between 2500 and 2700 m/s in several previous studies in the field of acoustics [41–43].

Sylgard 527 (Dow Corning) is used as the surrogate material for the brain tissue in the BIPED headform. The choice of Sylgard as brain tissue surrogate was driven by numerous factors, including the density match, the ease of manufacturing, the possibility of embedding instrumentation in the brain, and the availability of characterization data. A density match was deemed important to obtain an appropriate brain weight, which may influence the brain motion. The density of Sylgard is $975 \, \text{kg/m}^3$ compared to $1040 \, \text{kg/m}^3$ for brain tissue [6]. The longitudinal wave speed in Sylgard 527 has been estimated between 960 and 1050 m/s in previous studies [44,45]. This has also been verified experimentally with the BIPED headform where the delay between two successive transducers has been repeatedly measured [33]. There is a significant difference in sound speed (and bulk modulus) between Sylgard and brain tissue, the sound speed in brain tissue being estimated around 1560 m/s [46].

The differences in longitudinal wave speed and modulus of the skull and brain compared to their biological counterpart are limitations of the current model. However, the magnitude of the ratios between the two materials is adequate. It is expected that the lower stiffness of the skull surrogate may enhance the magnitude of skull deformation caused by the blast. Conversely, the lower modulus and wave speed of the Sylgard may cause the stress waves to attenuate more rapidly compared to brain tissue.

The BIPED is instrumented with five external flat pressure transducers, a customizable number of intra-cranial pressure transducers and, if required, a six-accelerometer package at the top of the neck.

The external flat pressure transducers provide information on the OP field history around the headform. They are positioned on the forehead, right side, left side, back, and top of the head. Kulite LL-125 piezo-resistive thin-line pressure transducers were selected to allow surface mounting. The transducers are modified from their standard configuration by having the protective screen over the diaphragm removed in order to maximize the sensor bandwidth.

Intra-cranial pressure transducers are carefully positioned into the brain mould before casting. Positioning is verified under X-ray imaging once the curing of the gel is completed (see Fig. 4b). The number and position of ICP transducers is typically adapted to the purpose of the different trials. Kulite XCL-072 pressure transducer series was found to be very reliable in terms of response and durability. In order to maximize the transducer bandwidth and repeatability, the protective screen over the diaphragm was removed as well. This also allowed the gel to fill any voids and guarantee an intimate contact between the gel and the sensing element of the transducer. The required bandwidth for these transducers was assumed to be less than that for the external transducers, since the waves travelling in the brain material are expected to be low-magnitude stress waves, as opposed to a shock wave.

While the selected ICP transducers are considered unidirectional, the deviatoric components of stress in the brain will be orders of magnitudes lower than the hydro-static component, due to the nature of the material. (The Poisson's ratio is close to 0.5.) Hence, the measurement should be relatively insensitive to gauge orientation for angles where the gauge itself does not interfere with the wave propagation direction.

A single headform is typically used for 20 detonations before being replaced. It was observed through several test series that after approximately 20 detonations, the seal of the skull begins to break and fluid starts to leak during the experiments. Also, a higher rate of sensor failure was observed after 20 tests on a headform. Throughout a test series, sensor mounts and skull joint integrity are regularly checked. The BIPED was successfully used in blast tests with static OP ranging from 40 to 350 kPa.

2.2 Blast from above-ground free-field trial

A full-scale free-field explosive trial was held at the Munition Experimental Test Center site located on the Canadian Force Base in Valcartier in 2011. The site is a large open area with a test section consisting of a concrete pad of 15 m × 15 m. The blast wave was generated using 5 kg of C4 explosive. A cylindrical charge, with a 1/1 diameter-to-height ratio, was centrally detonated using a C8 detonator. The charge was supported at the centre of the test pad using a sacrificial cardboard tube to a height of burst (HoB) of 1.5 m (centre of charge to ground). Two BIPED headforms were deployed at a constant radius of 5 m around the explosive charge along with two reference static OP gauges. Dynamic OP history was not measured in these experiments. However, measurements of surface OPs directly on the headform provided a full characterization of the applied loading.

The reference gauges and headform were mounted on support structures made of hollow steel posts, filled with urethane to mitigate transmission of ground vibrations. All structures were bolted into the concrete pad. The sensing element on the reference gauges and the nose of the headforms were adjusted to a height of 1.5 m. The reference gauges were large profiled discs instrumented with PCB 113b24 piezoelectric sensors mounted at the centre of the disc using stress relieved delrin inserts.

The positions of the ICP transducers are indicated by the blue dots in the radiographs of Fig. 5. Two pairs of transducers were cast in the brain parallel to the sagittal plane. Two transducers were positioned in the frontal lobe, mid-way between the front and centre of the brain, and two transducers were positioned halfway between the front and back surfaces. All transducers were positioned approximately 15 mm from the sagittal plane.

Raw signals from all reference and headform transducers were acquired at a sampling frequency of 500 kHz.
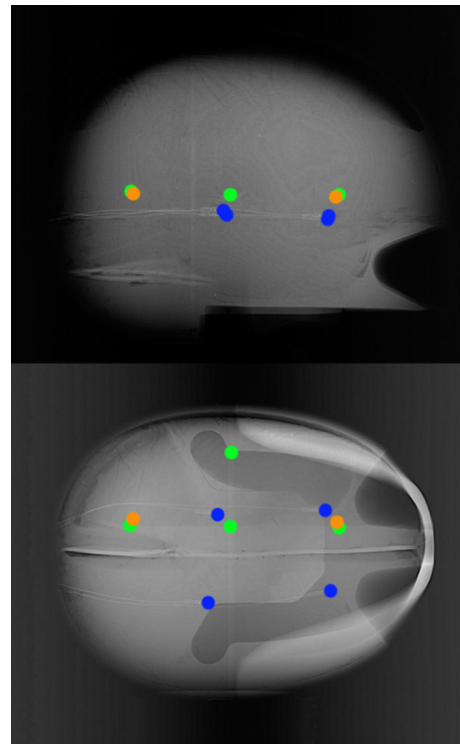

Fig. 5 Right lateral and craniocaudal X-ray image showing the positions of ICP transducers for each individual trial. Blue: above-ground trial, orange: near-ground and breaching trials, green: shock tube trial

Reference and BIPED external OP signals were typically post-processed using an 8-pole Butterworth phase-less low-pass filter at a cut-off frequency of 50 kHz. ICP signals were post-processed using the same filter but with a cut-off frequency of 10 kHz. Each individual test condition was repeated three times to perform an assessment of the level of repeatability of the blast profile and the headform response.

Figure 6 shows the reference static OP histories from three individual repeats of the test. Signals were synchronized on the time of arrival of the first shock. The general wave structure was characteristic of an air burst. It displayed three distinct shocks: the incident shock, the ground-reflected shock, and a secondary shock caused by gas recompression near the blast source. In this test configuration, the headform and reference pressure transducers lay above the intersection point between the Mach stem, the incident wave, and the reflected wave. The transducers therefore recorded an overlapping, double-peak wave structure. The peak static OPs were 90.28 kPa (SD = 2.37 kPa) and 110.54 kPa (SD = 2.47 kPa) for the incident and reflected waves, respectively. The total positive phase duration, taken from the initial pressure rise to the first crossing of the abscissa, was 5.37 ms (SD = 0.05 ms)

The original decision of using an air burst to study the response of the BIPED to a free-field blast was motivated by the desire to obtain a perpendicular blast flow relative to
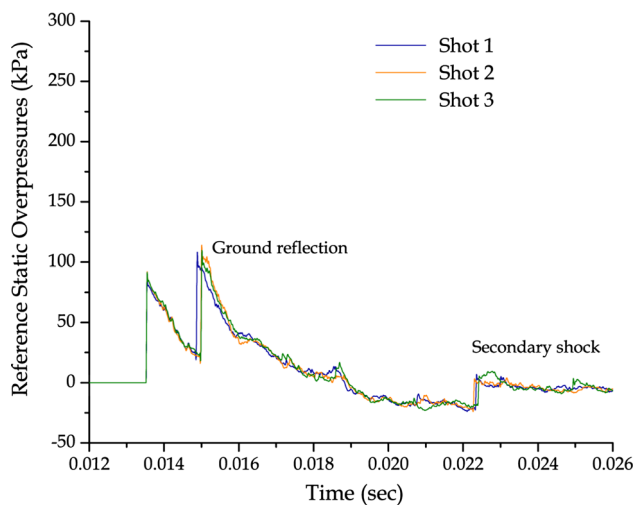
Fig. 6 Reference static overpressure history from free-field blast experiment with 5 kg of C4 (HOB = 1.5 m) at 5 m standoff
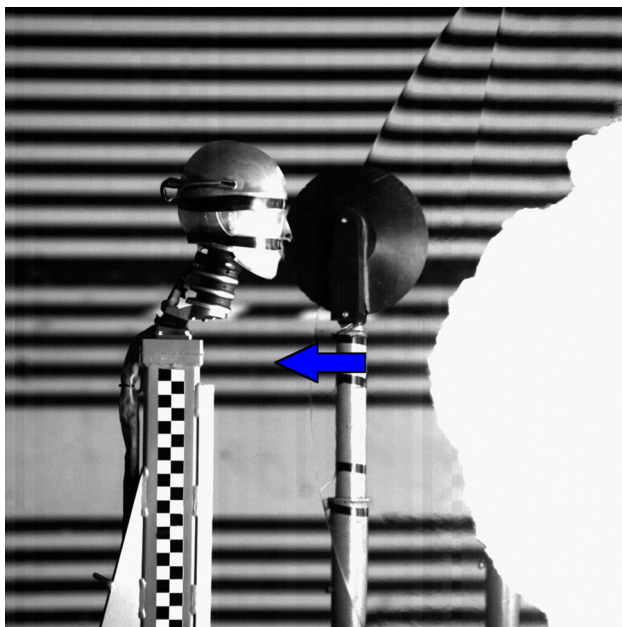

Fig. 7 Frame of high-speed video recorded from free-field blast experiment with 5 kg of C4 (HOB = 1.5 m) at 5 m standoff

the head. Figure 7 shows a frame from a high-speed video recorded during one of the tests. The incident shock could be distinctively observed along with the direction of propagation, indicated by the blue arrow. There was still significant curvature of the shock at the point of loading. The direction of propagation of the ground reflected wave was approximately 45° relative to the incident wave.

2.3 Blast from near-ground free-field trial

A second free-field blast trial was held at the Munition Experimental Test Center (METC) site on the Canadian Force Base
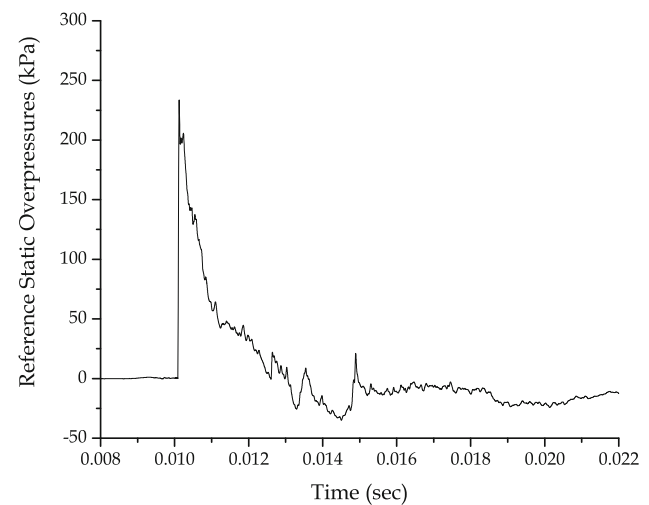
Fig. 8 Reference static overpressure history from free-field blast experiment with 5 kg of C4 (HOB = 0.2 m) at 4 m standoff

in Valcartier. The general setup was similar in almost every aspect to the above-ground free-field trial. The only difference was the height of burst, which was lowered to 0.2 m in order to simulate a surface burst, and the standoff distance, which was set to 4 m. Standoff was measured from the centre of the charge to the nose of the headforms.

The positions of the ICP transducers within the headform are shown as the orange dots on the X-ray images from Fig. 5. Two transducers were cast into the brain on the right side of the sagittal plane. The first transducer was positioned in the frontal lobe, and the second transducer was positioned at the back of the parietal lobe, facing backwards. The two transducers were positioned 15 mm from the sagittal plane and 10 mm above the top of the orbital cavity. The sampling frequency of all transducers was increased from 500 kHz to 1 MHz. Figure 8 shows the reference static OP histories from a single test of the near-ground trial. The average peak pressure obtained over three repeated experiments was 233.55 kPa (SD = 20.40 kPa), and the average positive phase duration was 2.5 ms (SD = 0.11 ms).

The wave structure was observed to be a single main shock followed by a short negative phase and a smaller amplitude secondary shock. The direction of propagation of the main blast wave was not perpendicular to the forehead, but oblique and upward at approximately 30°. Figure 9 shows a frame taken from a high-speed video recorded during a test. The direction of propagation is indicated by the blue arrow. This loading condition provided an opportunity to study the influence of parameters such as the height of burst and standoff distance on the headform response.

2.4 Shock tube trial

A shock tube trial was held at the TNO (the Netherlands Organisation for Applied Scientific Research TNO) Rijswijk
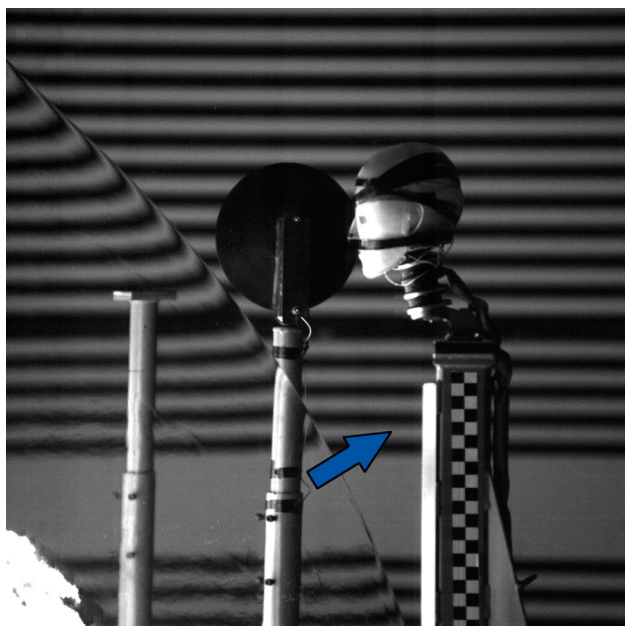
Fig. 9 Frame of high-speed video recorded from free-field blast experiment with 5 kg of C4 (HOB = 0.2 m) at 4 m standoff
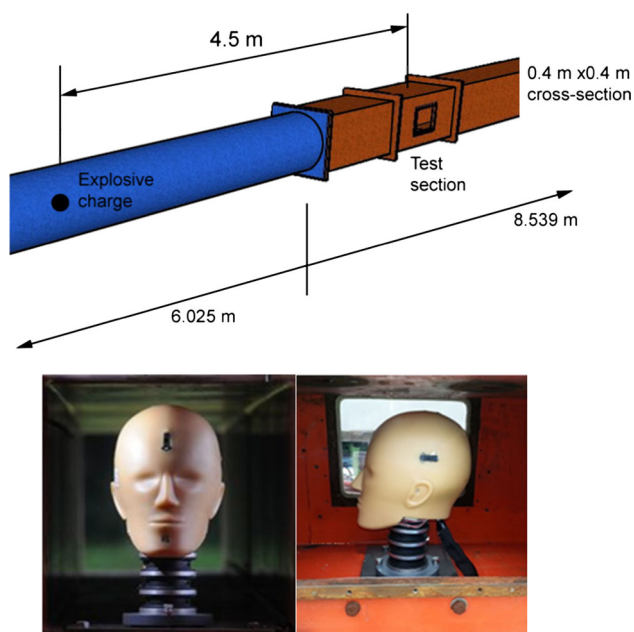

Fig. 10 TNO explosively driven shock tube test configuration

facilities in the Netherlands. The shock tube consisted of an open-ended cylindrical driver section connected to an open-ended square tube of 0.400 m × 0.400 m in cross section. The test section was located in the square section, 4.5 m away from the explosive charge used to generate the shock wave. The length of the driver section was 6.025 m, and the length of the tube was 14.564 m (Fig. 10).

The driver section consisted of two parts which can be split to insert the explosive charge. A window on both sides

of the test section allowed for the installation and observation of the headform. Two reference pressure transducers were flush mounted on the side wall at a distance of 350 and 150 mm ahead of the headform. They were used to monitor the static OP of the incident shock wave during the experiments. The transducers were Endevco, type 8530C-100, with an operational range of 0–690 kPa. All signals from the reference transducers and from the headform were sampled at 1 MHz.

The shock wave was generated by detonating a spherical charge of 7 g of C-4 explosive, at the centre of the driver cross section. The BIPED headform was mounted on a HIII neck. The neck was then mounted on a custom-made bracket allowing rotation of the headform around the vertical axis. After setting, the neck was secured by two bolts at the bottom of the tube.

The headform used during the shock tube trial was instrumented with four ICP transducers in the left brain hemisphere. They were, respectively, positioned in the frontal lobe, temporal lobe, front of parietal lobe, and back of parietal lobe. Positions are illustrated by the green dots in Fig. 5. The transducers in the frontal lobe and at the front of the parietal lobe were oriented towards the front of the headform. The transducers at the back of the parietal lobe and in the temporal lobe were, respectively, oriented towards the back and left side of the head.

This experimental arrangement was selected to investigate the response of the headform under loading conditions similar to those used in many laboratories performing research on blast neuro-trauma. These conditions were not expected to be representative of free-field blast conditions or of a blast typically encountered in military operation. Indeed, the test configuration was expected to produce a much higher dynamic pressure due to the high ratio of blockage, which is estimated at approximately 30% and which is well above the recommended blockage ratio of 5% [23]. The higher dynamic pressures combined with the longer duration of the positive phase create a drag force of a magnitude and duration which are probably not experienced in free-field scenarios.

The tube at TNO has the advantage of being very long, which allows for any rarefaction wave travelling back into the tube from the open-end to be clearly separated in time (approximately 20 ms after the end of the initial positive phase). This is convenient when testing with a surrogate as the analysis can focus on the relevant timeframe and ignore the loading artefacts occurring at a later time.

The shock tube generated a highly repeatable OP history. Figure 11 shows an example of side wall OP history from a calibration test done without target. The obtained peak static OP was 79.2 kPa and the positive phase duration was 8.56 ms.
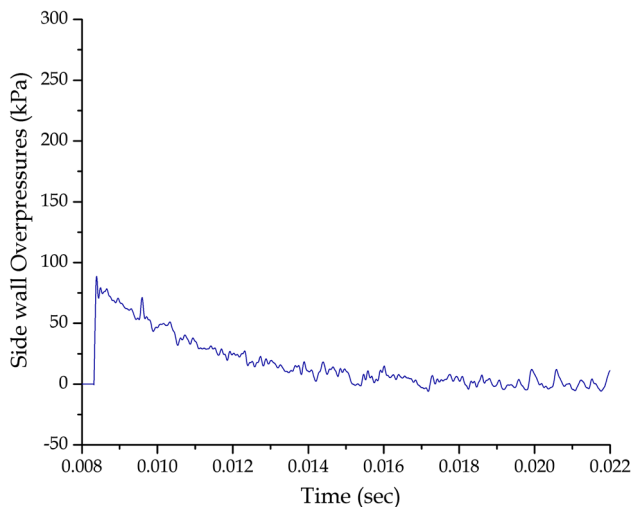
Fig. 11 Reference side wall overpressure history at 4.35 m down the tube from the point of detonation, for shock tube experiment using 7 g of C4 with no target
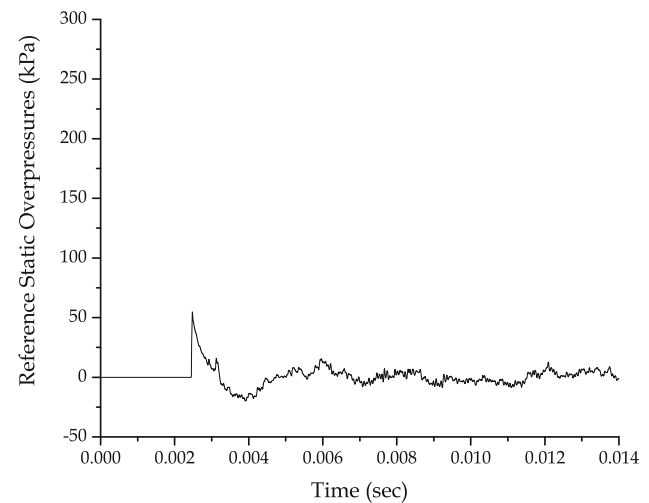

Fig. 13 Reference static overpressure history from breaching blast experiment using 15 g of PETN detonation cord at 1.25 m standoff
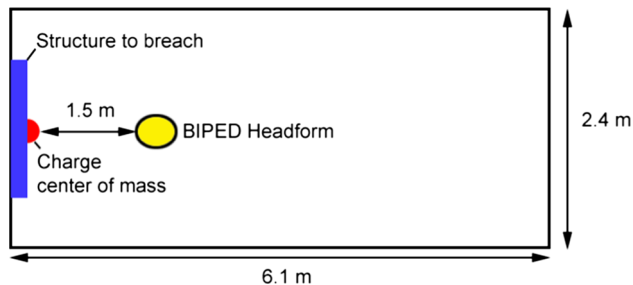

Fig. 12 Schematic of test setup for the breaching trial held in the near-ground trial (top view)

2.5 Breaching trial

A blast trial simulating a breaching exercise was carried out inside a closed room of approximately 2.4 m by 2.4 m by 6.1 m. The structure to be breached was at one end of the room and was approximately 1 m by 1.25 m. The blast wave was generated using 15 g of PETN detonation cord, laid-out symmetrically around the opening. A schematic of the trial setup is shown in Fig. 12. The red hemisphere represents the centre of mass of the detonation cord layout.

The BIPED headform was positioned facing the explosive with a standoff of 1.5 m. The height of the nose of the headform was aligned with the centre of mass of the explosive, at 1.5 m from the floor. The headform used in this trial is the same as the one deployed in the near-ground free-field trial. It had two ICP transducers cast in the frontal and parietal lobe, as shown by the orange dots in Fig. 5. The transducer in the parietal lobe was facing the back of the head.

Tests were also carried out without a target in order to characterize the static OP history at the target location. This was done by using a custom blast pencil instrumented with a

PCB 113B24 piezo-electric sensor. The blast pencil was positioned so that the sensing element was at the same height as the nose of the headform in subsequent tests. Signals from both the headform and the blast pencil were sampled at 1 MHz.

Figure 13 shows the reference static OP history obtained from a test without a headform. The peak static OP was 54.8 kPa, and the positive phase duration was 0.77 ms. The OP distinctively dropped towards the end of the positive phase due to the successful breaching of the opening, which introduced a rarefaction wave into the chamber. Although the blast pencil was oriented towards the blast source, the transducer was not expected to measure the static OP for the entire duration of the measurement. Reflections from the chamber walls and ceiling generated a flow field that does not necessarily remain parallel to the instrument. The OP history of Fig. 13 is shown to provide a sense of scale when comparing the initial peak with the other test conditions presented previously. The external pressure field history obtained from the headform was considered a more appropriate representation of the loading conditions.

In the present study, the four independent trials introduced above generated reasonably different loading conditions on the headform. They were expected to generate a response with different relative contributions from the direct and indirect biomechanical pathways. For example, the blast generated from the shock tube had a positive phase duration 60% longer than that of the above-ground free-field trial. The total impulse obtained from the shock tube experiment was greatly enhanced by the excessive flow blockage. It was expected that this feature would dominate the loading history and generate significant global motion of the headform. In contrast, it was expected that blast generated during the breaching trial

would have a much smaller total impulse that may not be sufficient to create much global motion.

2.6 Repeatability of results

In every trial, each test condition was repeated three times. The repeatability of the loading conditions and the headform response was assessed. For the purpose of this article, assessment of repeatability is only provided for the above-ground trials. Levels of repeatability were comparable in all four trials discussed herein.

Figure 6 shows that the level of repeatability of the generated blast was satisfying. For bare explosive charge trials, this was mainly attributed to extreme attention to detail during the charge casting and preparation process, the detonator insertion, the charge support method, and the reference transducer positioning. Finer details in the wave decay phases also display a good level of repeatability. The time of arrival of the reflected wave, which varied by about 0.2 ms between shot 1 and the other shots, was the most observable variation in the main wave structure. It was unclear what might have caused this delay, but it was considered of minor importance and should not have a great impact on the headform response.

Figure 14 shows an example of the level of repeatability obtained for the BIPED external OP measurements. The level of repeatability was similar to that of the reference pressure gauges, which suggests that the BIPED transducers were reliable and did not introduce additional sources of variability. The observed variability in the time of arrival of the ground reflection was also noticeable in the forehead OP signals. Similar repeatability was obtained from the side and back external OP transducers (not shown), which further suggests that the interaction of the blast wave with the headform and the evolution of the surrounding OP field is reproducible.
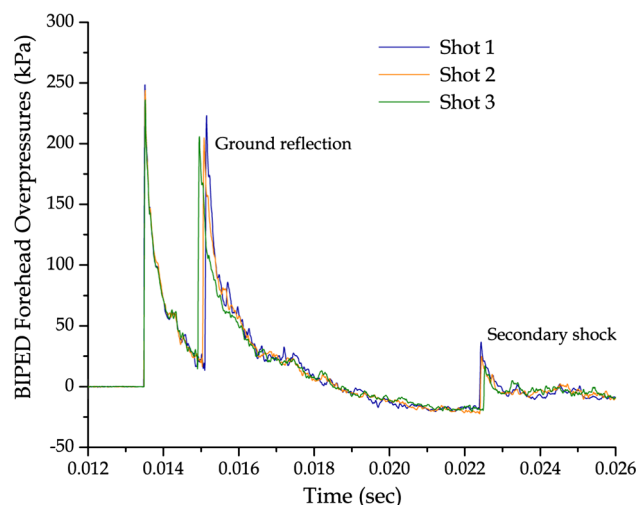

Fig. 14 BIPED forehead overpressure history from free-field blast experiment with 5 kg of C4 (HOB = 1.5 m) at 5 m standoff
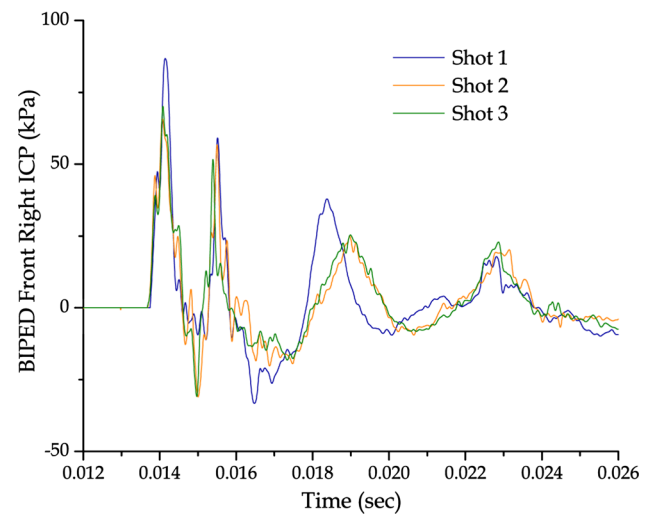

Fig. 15 BIPED front ICP history from free-field blast experiment with 5 kg of C4 (HOB = 1.5 m) at 5 m standoff

However, the complexity of the interaction between the blast wave and the headform may introduce local variations in loading on sections of the head that are not covered by the instrumentation.

Figure 15 shows the front ICP signals from the same three repeats discussed above. The variability was slightly higher when compared with external OP, in terms of both peaks and other minor fluctuations. However, the general wave structure was similar.

A potential source of variation was the initial position of the brain within the skull. There was no way of guaranteeing that the brain recovered its exact initial position after a test. Small variations in the initial position of the brain before a test may have been responsible for the increase in variability in the ICP. It was also expected that the complexity of the interaction between different ICP waves could introduce variations between repeats. Repeatability is critical when comparing different loading scenarios, as the hope is that the difference in the headform response can be confidently attributed to the difference in loading condition, not simply variability.

2.7 Validation of external transducer output

The bandwidth requirement for transducers meant to measure peak blast OP is not precisely defined. In order to further validate the measurements obtained from the reference and BIPED external transducers, the shock velocity measured during the above-ground blast trial was used to calculate the expected peak static OP and peak reflected OP.

For the case of a free-field blast wave travelling in air ($\gamma = 1.4$), the incident OP can be calculated using the following relationship, derived from the conservation equations at the shock front [47]:
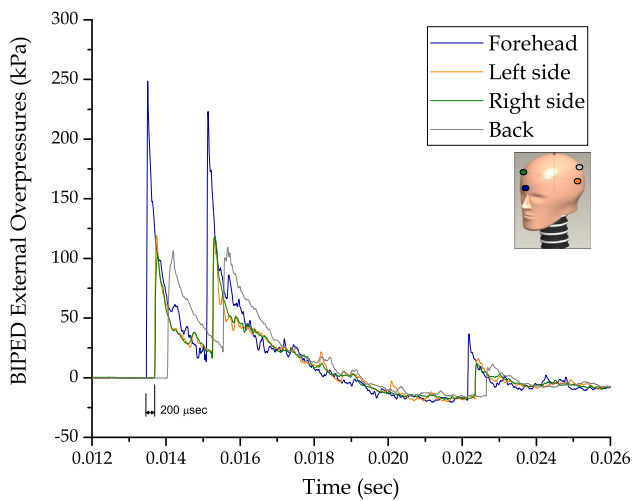
Fig. 16 BIPED external overpressure field history from free-field blast experiment with 5 kg of C4 (HOB = 1.5 m) at 5 m standoff

$$\Delta P = \frac{\left(\left(\frac{U}{c_0}\right)^2 - 1\right) * 7 P_0}{6},\tag{1}$$

where ΔP is the peak static OP, P_0 is the ambient pressure (99.8 kPa), U is the shock velocity, and c_0 is the ambient acoustic speed (338 m/s). Similarly, for a blast wave that reflects perpendicularly on a rigid surface, the peak reflected OP is given by:

$$P_{\text{ref}} = 2\Delta P \left(\frac{7 P_0 + 4\Delta P}{7 P_0 + \Delta P}\right).\tag{2}$$

Using the shock velocity estimated from the delay between the forehead and side OP transducer in Fig. 16 (200 µs), a shock velocity of 450 m/s was found. Equation (1) yielded a static peak OP of 89.9 kPa. This was less than 1% lower than the average peak measured using the reference pressure gauges. For the same test, (2) yielded a peak reflected OP of 242.6 kPa. Again, this was less than 1% lower than the average peak forehead OP measured on the BIPED. While the head is not a semi-infinite flat and rigid surface, it is not surprising to observe that the instantaneous reflection of the incident wave on the forehead creates a peak OP similar to the perfectly reflected peak OP predicted by (2). These results suggested that the transducers have sufficient bandwidth to resolve peak static and reflected OP.

3 Results and discussion

3.1 Above-ground free-field trial

A few interesting features were observed in the external OP field measurement around the headform (Fig. 16). First, the

highest loads occurred on the front of the head, where the incident and ground-reflected shocks were reflected by factors of 2.69 and 1.91, respectively. The lower reflection ratio of the ground reflection was due to the different propagation directions. The incident wave experienced a near perpendicular reflection, whereas the ground reflection experienced an oblique reflection. Second, the side peak OPs were slightly higher than the reference static peak OP. This was due to the sides of the headform not being perfectly parallel to the blast flow. The side measurements were symmetric, validating that the headform was perfectly aligned with the blast source. Third, the back peak OP was very close to the reference peak static OP. This was in contrast with the notion that a blast wave diffracting around a head eventually merges and superposes at the back of the head. However, this local phenomenon might still have occurred millimetres away from the transducer location. Finally, the transit time of the blast wave from the forehead to the back was approximately 450 µs, while equilibrium in the external OP field was reached after approximately 3.5 ms.

The corresponding frontal and centre ICP signals appeared to follow the loading profile of the forehead quite well for the first 3 ms (Fig. 17), after which a delayed third peak was observed. The ICP signals were relatively damped compared with the external blast wave and were more characteristic of stress waves than shocks. The frontal lobe experienced an initial peak ICP on the order of 35% of the forehead overpressure. This was found to be similar to other transmission factors reported from cadaveric experiments in the literature [1,39]. The concordance of the timescale and magnitude of the first two peaks of ICP with the forehead OP suggests that the stress waves mainly originated from the front of the head. We noted that the delay between the initial rise of frontal and centre ICP was between 0.06–0.07 ms. The wave velocity
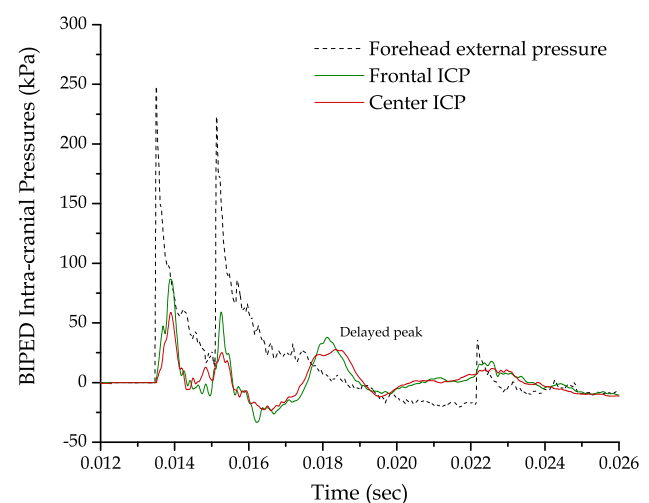

Fig. 17 BIPED ICP history from free-field blast experiment with 5 kg of C4 (HOB = 1.5 m) at 5 m standoff

was therefore estimated between 857–1000 m/s, which is in accordance with the reported acoustic velocity in Sylgard 527 [45, 46].

The delayed third peak on the ICP signals was observed when the external pressure field was nearly in equilibrium. This peak had a much longer rise time than the first two peaks. Indeed, the third peak had a characteristic frequency around 500 Hz, while the first two were over 1200 Hz. The high-speed imagery taken during the test showed that the third peak occurred when the global displacement of the headform reached a maximum. It is believed that the third peak could be a consequence of the lagging motion of brain relative to the skull. The brain could have experienced increased contact forces as the head moved backward. Another possibility is that this peak was the result of a mode of skull deformation of lower natural frequency, which occurred when the external OP field reached equilibrium.

The three peaks in the ICP signal were of comparable magnitude. While the first two peaks appeared to be caused by a more direct biomechanical pathway, the third peak was potentially the result of an indirect one. Interestingly, the high and low characteristic frequencies present in the signal were similar to those identified previously [28] and pertaining to local skull deformation and relative brain-to-skull motion, respectively.

3.2 Near-ground free-field trial

For the near-ground free-field blast condition, the external OP field (Fig. 18) agreed well with the reference OP history. Compared with the above-ground blast trial, this condition created an OP at the forehead with a single peak of higher amplitude (590 kPa) and a much shorter positive duration
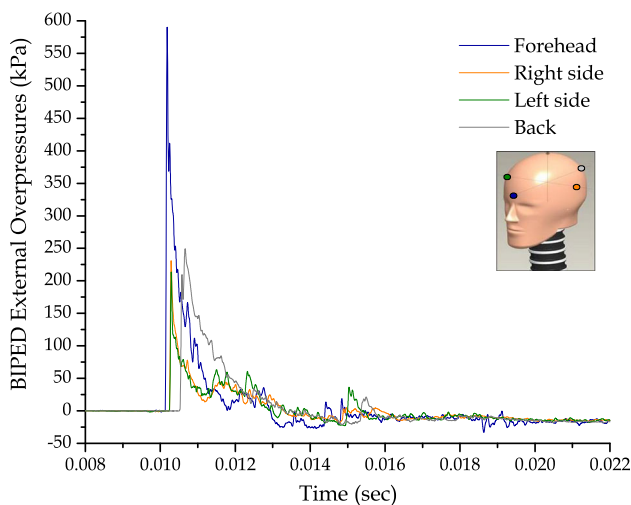

Fig. 18 BIPED external overpressure field history from free-field blast experiment with 5 kg of C4 (HOB = 0.2 m) at 4 m standoff
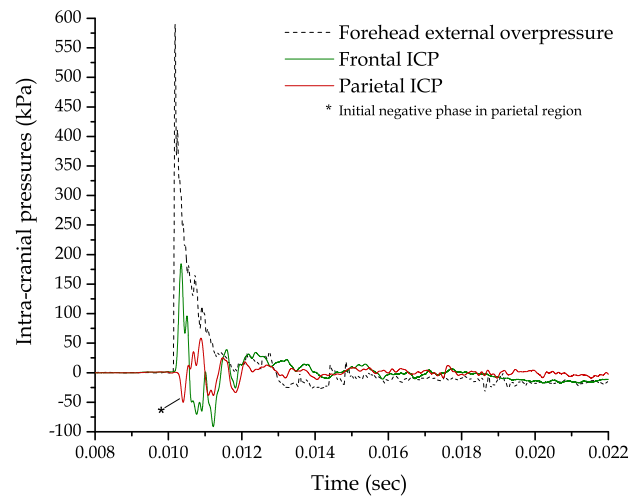

Fig. 19 BIPED ICP history from free-field blast experiment with 5 kg of C4 (HOB = 0.2 m) at 4 m standoff

(2.8 ms). The reflection factor was, however, of a similar order of magnitude (2.53). Due to the propagation direction of the blast wave, this condition created larger pressure gradients between the front, back, and sides of the head. The delays between the rise of the front, sides, and back overpressures were also changed. These results provided evidence that for a similar charge size, the height of burst has a significant influence on the evolution of the loading on the head.

Again, the early-time frontal ICP variations followed the loading profile on the forehead (Fig. 19). The magnitude of the ICP peak reaches 31% of the external peaks in the frontal lobe, which is of the same order of magnitude as was observed in the above-ground blast trial. However, there was a more noticeable negative phase in the frontal ICP signal. The negative phase was potentially the result of the elastic rebound of the skull, helped by the release of OP at the front and the rise of the OP at the back of the skull.

The parietal ICP (Fig. 19), which was not monitored in the above-ground trial, provided additional evidence of skull flexure. The initial parietal ICP response was negative, indicating that tensile stresses are being developed first at the back of the head. This negative ICP was observed prior to the arrival of the external shock at the back of the head. We observed that the most probable pathway for a stress wave to reach the back of the brain and generate a tensile stress state was through the skull material. Furthermore, the delay between the rise of the frontal ICP and the parietal ICP agrees with the wave transit time through the skull. Compression waves initiated at the front of the skull travelled through the skull and towards the back of the head. Upon reaching the free surface of the skull, these waves are reflected as tensile waves that locally pull on the skull, generating tensile stress wave in the underlying region of the brain. The blast wave transit time around the head was also important. The negative

phase in parietal ICP ended at the same time as the external OP at the back of the head started rising. Most importantly, the main frequency in the first few oscillations in frontal ICP and parietal ICP was, again, approximately 1200 Hz. Both ICP signals synchronized shortly before the external OP field equilibrated.

Even though the total positive impulse on the front of head was similar between the near-ground and above-ground blast exposure conditions, there were no clear signs of a delayed lower-frequency peak. Such a peak may have been hidden within the higher-magnitude, higher-frequency oscillations. However, this condition did appear to cause less displacement of the head. The results suggested that the energy partitioning between potential direct and indirect biomechanical pathways was different for this exposure condition.

3.3 Shock tube trial

In addition to creating a lower peak OP and longer positive phase duration at the forehead (208.1 kPa, 7.5 ms, reflection factor of 2.63), the loading conditions from the shock tube created an external OP field history, which evolved very differently from those obtained with the free-field blast conditions (Fig. 20). The decay phase of the forehead, side, and back OP was greatly affected by the high ratio of blockage in the tube and the resulting turbulent flow field. Restricting the blast flow in the tube prevented the blast wave from diffracting around the headform as it would have in a free-field environment, effectively increasing the dynamic pressure component of the loading. Another unique aspect of the external OP field obtained in the shock tube is that the back OP never significantly surpasses the OP at the forehead. The OP field reached near-equilibrium 3 ms after the initial shock
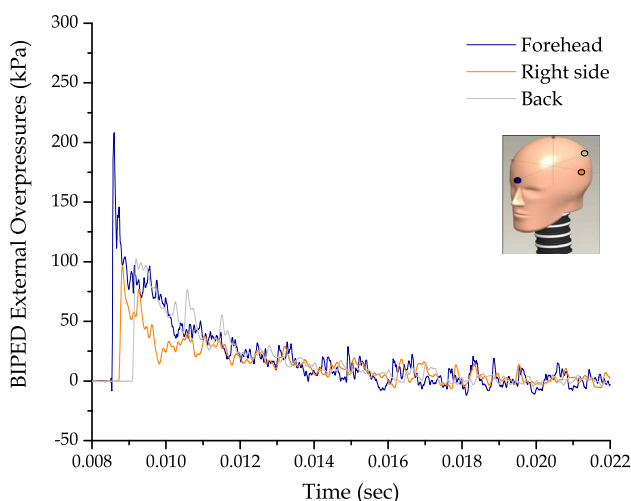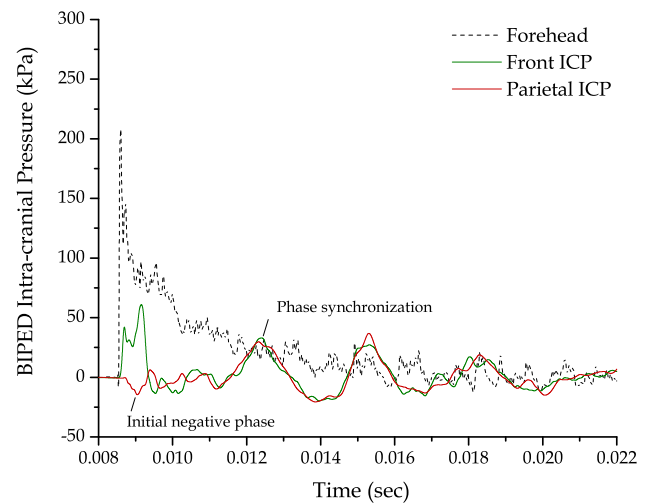

Fig. 21 BIPED ICP history from shock tube experiments

rise, after which a positive OP field remained for more than 5 ms.

This particular OP field resulted in an equally distinctive ICP response (Fig. 21). The early frontal ICP response followed the applied forehead OP, in a manner similar to the aforementioned trials. The parietal ICP signal also started with a tensile phase which was again approximately 1/3 of the magnitude of the positive ICP at the front. However, both ICPs showed apparent and sustained delayed oscillations with a characteristic frequency of approximately 350 Hz. This second phase of ICP fluctuation started after 3 ms, when the external OP field had reached equilibrium. The shock tube loading condition appeared to cause a magnification of later-time oscillations, suggesting that the partitioning of energy between the different modes of response had been changed.

The expected increase in dynamic pressure and the larger impulse on the BIPED should enhance the global motion of the BIPED. This was confirmed by the high-speed imagery, where significant translational and rotational head motions were observed. It appeared natural to associate the low-frequency oscillations to the global motion of the headform, and more precisely to the relative motion of the brain with the skull. However, the possibility of a low-frequency, synchronous mode of skull deformation cannot be discounted.

3.4 Breaching trial

The breaching trial generated loading conditions that were at the other end of the spectrum when compared with the shock tube trial. The OP applied to the forehead had a lower peak and much shorter duration (160.3 kPa, 0.7 ms, reflection factor of 2.92). The distinctive feature in the external OP field history was that the OP field never reached equilibrium before the pressure returned to near ambient condition (Fig. 22). The
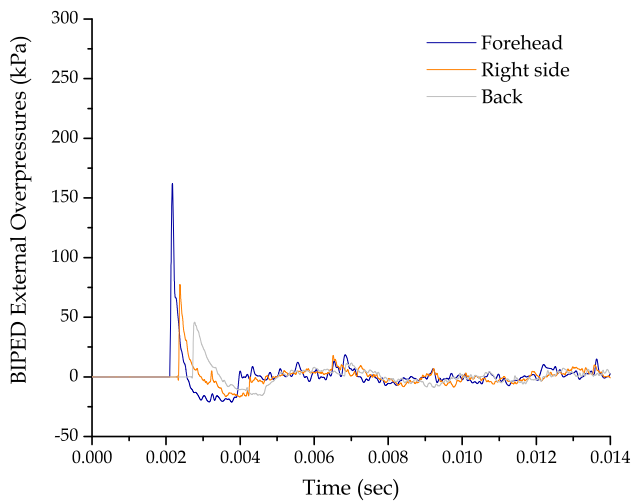

Fig. 20 BIPED external overpressure field history from shock tube experiments

Fig. 22 BIPED external overpressure field history from breaching trial

Fig. 23 BIPED ICP history from breaching trial

loading was considerably more directional, as the forehead OP was already in a negative phase when the OP increased at the back of the head.

The frontal ICP signal showed the expected initial rise which followed the forehead OP. As with the previous trial, the parietal ICP showed an early negative phase with a magnitude of approximately 1/3 ratio of the positive frontal ICP (Fig. 23). The interesting feature of the parietal ICP was that the first cycle is followed by a few more cycles of oscillations at the characteristic frequency of approximately 1000 Hz. Moreover, the magnitude of this oscillation appeared to increase slightly. This may have been due to a unique timing between the elastic rebound of the skull and the arrival of the external blast wave at the back of the head. After an initial compressive wave travelled in the skull simulant to put the back of the skull in tension, the skull likely rebounded at the same time as the external blast wave loaded the back of the head in compression. The tension–compression oscillation seen in the parietal ICP was likely further encouraged by the negative phase of OP at the forehead. Both ICP signals showed no signs of delayed low-frequency peaks. The direct biomechanical pathways appeared to dominate the ICP response for the breaching loading condition.

4 Discussion

Based only on the evidence presented above, one may still wonder about the origin of the lower-frequency oscillations observed in the above-ground free-field trial and the shock tube trial. They could have been the result of brain-to-skull relative motion, but also a manifestation of a lower mode of skull deformation. Additional tests carried out during the above-ground free-field trial and the shock tube trial, where
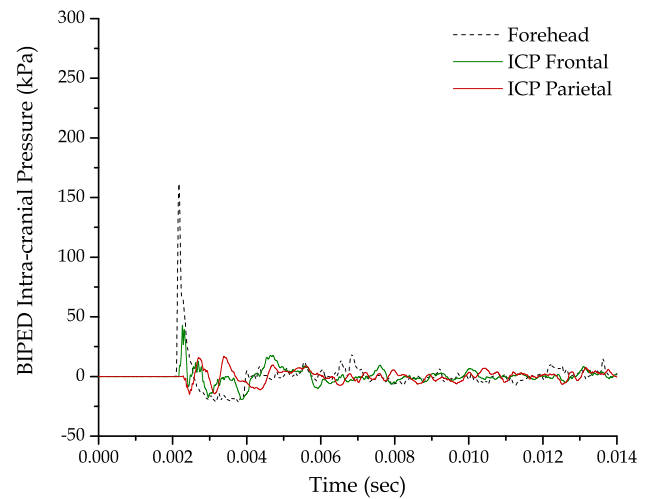
full-face helmets were tested on the BIPED, shed light on this question. While the full-face helmets were able to significantly reduce early peaks in ICP, they were ineffective at reducing the later-time oscillations. Moreover, delayed peaks were enhanced by the presence of the full-face helmet in the above-ground free-field trial. It appears very unlikely that the delayed fluctuations were caused directly by a natural mode of deformation of the skull, as the helmets have proved to significantly reduce the response from this pathway.

The reanalysis of BIPED external OP and ICP signals from four different blast wave experiments proved that the headform response was highly dependent on the loading characteristics. The energy partitioning between the different modes of response of the headform can change depending on multiple factors: the magnitude of the peak OP, the blast wave structure, the direction of propagation, the positive phase duration, and the timing of the external blast wave relative to the propagation of stress waves in the skull.

To better illustrate the notion of partitioning between direct and potentially indirect biomechanical pathways, the energy spectral density (ESD) of the frontal ICP signal was computed for all four conditions. The ESD gives information with regard to how signal energy is distributed along the frequency spectrum of that signal. An example of such spectrum is shown in Fig. 24, where it can be seen that for the above-ground test condition, the signal energy is mostly found below 2000 Hz (90%). Approximately half of the energy in the signal is found below 750 Hz.

The ESD cumulative sum ratio, defined as the integral of the ESD normalized over the total energy in the signal, was also calculated for all four test conditions. The resulting curves are shown in Fig. 25. The curves show how the cumulative ratio of the signal energy evolves with increasing bandwidth from 0 to 5000 Hz. A sharp rising curve indicates that there is a large proportion of the energy within a specific
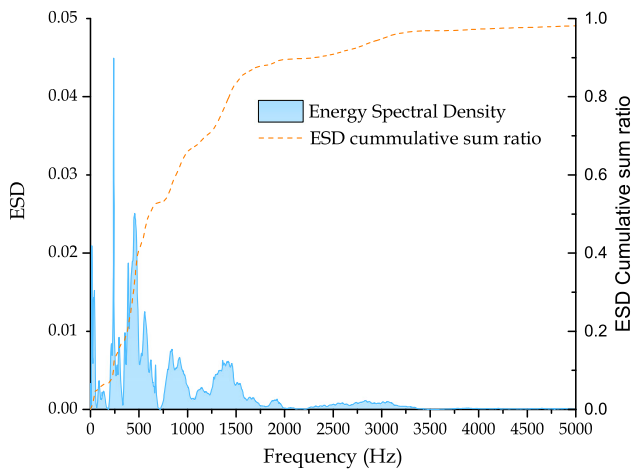
Fig. 24 Energy density spectrum (ESD) and ESD cumulative sum ratio for the above-ground free-field test condition
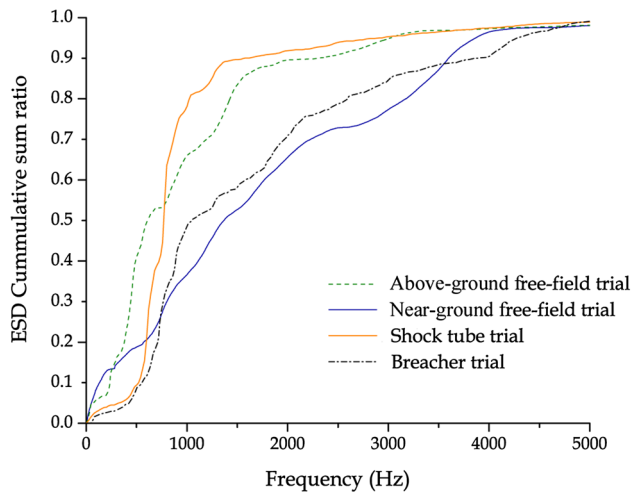

Fig. 25 Energy density spectrum (ESD) and ESD cumulative sum ratio for all four test conditions

scaling of the brain and skull as well as by including a CSF simulant and membranes to constrain brain motion. However, the BIPED lacks a spine structure and it is currently difficult to estimate whether the BIPED brain is constrained more or less than a human brain. This does not invalidate the findings reported here, which demonstrated that several loading characteristics play a critical role in soliciting different modes of response in the head.

Further understanding of these modes of response is not only crucial to the design of effective protective systems, but also instrumental to the determination of criteria and thresholds linking exposure characteristics to an injury outcome.

Follow-on work currently focuses on improving the BIPED instrumentation suite to include skull-mounted strain gauges and brain-to-skull contact force transducers. These should allow for an even better discrimination between the headform modes of response by linking directly skull deformation and brain-to-skull contact to ICP variations.

5 Conclusion

The BIPED headform, an instrumented physical model of the head comprised of a skin, skull, brain, membranes, and CSF, was deployed in different blast experiments which offered significantly different loading characteristics. By reanalysing and cross-comparing the BIPED external overpressure and intra-cranial pressure data from these experiments, it was shown that the BIPED response is multi-modal and that the energy partitioning between the different modes of response depended on the blast exposure characteristics. Strong evidence of direct biomechanical pathways, such as skull deformation, was presented. Evidence of indirect biomechanical pathways, such as relative brain-to-skull motion, was also presented. Results showed that the different mechanisms leading to the presence of stress waves in the brain are not mutually exclusive. They can occur within a single event and affect similar regions of the brain. These findings suggest that research aimed at defining exposure thresholds cannot focus on a single stress transmission mechanism in isolation, use experimental designs that are not representative of realistic blast loading scenarios, or focus on only one narrow set of blast conditions. Understanding of the injury mechanisms of blast neuro-trauma likely requires a more holistic approach where various operationally relevant blast loading conditions need to be considered simultaneously.

band, while a smooth rising curve indicates that energy is more dispersed across the spectrum.

The ESD cumulative sum ratios show that signal energy was the most dispersed for the breaching trial and the near-ground free-field trial. Concurrently, these were the two trials where global motion of the headform was the smallest. In the near-ground trial, there was slightly more content below 500 Hz, but the energy portion below 1000 Hz was still less than 40%. In the above-ground trial, a sharp increase in signal energy is found under 500 Hz and almost 65% of the total energy is now found below 1000 Hz. For the shock tube trial, this proportion jumps to nearly 80%.

A limitation of the presented work is that the level of constraint of the BIPED brain into the skull cavity was not calibrated against human data. The design attempts to reproduce the head structure and boundary conditions of the brain as much as possible. This is achieved by using appropriate

References

1. Courtney, A., Courtney, M.: The complexity of biomechanics causing primary blast-induced traumatic brain injury: a review of potential mechanisms. Front. Neurol. **6**, 221 (2015). doi:10.3389/fneur.2015.00221

2. Bass, C.R., Panzer, M.B., Rafaels, K.A., Wood, G., Shridharani, J., Capehart, B.: Brain injuries from blast. Ann. Biomed. Eng. **40**(1), 185–202 (2012). doi:10.1007/s10439-011-0424-0

3. Gupta, R.K., Przekwas, A.: Mathematical models of blast-induced TBI: current status, challenges, and prospects. Front. Neurol. **4**, 59 (2013). doi:10.3389/fneur.2013.00059

4. Young, L., Rule, G.T., Bocchieri, R.T., Walilko, T.J., Burns, J.M., Ling, G.: When physics meets biology: low and high-velocity penetration, blunt impact, and blast injuries to the brain. Front. Neurol. **6**, (2015). doi:10.3389/fneur.2015.00089

5. van Dommelen, J.A.W., Hrapko, M., Peters, G.W.M.: Mechanical properties of brain tissue: characterisation and constitutive modelling. In: Kamkim, A., Kiseleva, I. (eds.) Mechanosensitivity of the Nervous System, pp. 249–279. Springer, New York (2009). doi:10.1007/978-1-4020-8716-5_12

6. Brands, D.W.A., Peters, G.W.M., Bovendeerd, P.H.M., Wismans, J., Paas, M.H.J.W., van Bree, J.L.M.J: Comparison of the dynamic behavior of brain tissue and two model materials. In: SAE technical paper, 99SC21 (1999)

7. Bolander, R., Mathie, B., Bir, C., Ritzel, D., VandeVord, P.: Skull flexure as a contributing factor in the mechanism of injury in the rat when exposed to a shock wave. Ann. Biomed. Eng. **39**(10), 2250 (2011). doi:10.1007/s10439-011-0343-0

8. Moss, W.C., King, M.J., Blackman, E.J.: Skull flexure from blast waves: A mechanism for brain injury with implications for helmet design. Phys. Rev. Lett. **103**(10), 108702 (2009). doi:10.1103/PhysRevLett.103.108702

9. Bir, C.: Measuring blast-related intracranial pressure within the human head. DTIC report, ADA547306. http://www.dtic.mil/get-tr-doc/pdf?AD=ADA547306 (2011). Accessed 28 Aug 2017

10. Hua, Y., Akula, P.K., Gu, L., Berg, J., Nelson, C.A.: Experimental and numerical investigation of the mechanism of blast wave transmission through a surrogate head. J. Comput. Nonlinear Dyn. **9**(3), 031010 (2014). doi:10.1115/1.4026156

11. Varas, J.M., Philippens, M., Meijer, S.R., VanBree, J.L.M.J., deVries, D.V.W.M.: Physics of IED blast shock tube simulations for mTBI research. Front. Neurol. **2**, 58 (2011). doi:10.3389/fneur.2011.00058

12. Cooper, G.J.: Protection of the lung from blast overpressure by thoracic stress wave decouplers. J. Trauma Inj. Infect. Crit. Care **40**(3s), 105–110 (1996)

13. Courtney, A.C., Adrusiv, L.P., Courtney, M.W.: A test of the acoustic impedance model of blast wave transmission. J Battlefield Technol. **16**(3), 1–4 (2013)

14. Tikhonravov, A.V., Trubetskov, M.K., Winfree, N.A., Kang, J.H.: Low-frequency approximation of optimal elastic parameters for two-layer blast protection jackets. Num. Meth. Prog. **7**, 23–25 (2006)

15. Leonardi, A., Bir, C., Ritzel, D., Vandervord, P.: Intra-cranial pressure increases during exposure to a shock wave. J. Neurotrauma **28**, 85–94 (2011). doi:10.1089/neu.2010.1324

16. Ono, K., Kikuchi, A., Nakamura, M., Kobayashi, H., Nakamura, N.: Human head tolerance to sagittal impact reliable estimation deduced from experimental head injury using subhuman primates and human cadaver skulls. In: SAE technical paper 801303 (1980). doi:10.4271/801303

17. Zhang, L., Yang, K.H., King, A.I.: A proposed injury threshold for mild traumatic brain injury. J. Biomech. Eng **126**(2), 226–236 (2004). doi:10.1115/1.1691446

18. Hutchinson, J., Kaiser, M.K., Lankarani, H.M.: The head injury criterion (HIC) functional. Appl. Math. Comput. **96**, 1–16 (1998). doi:10.1016/S0096-3003(97)10106-0

19. Battacharjee, Y.: Shell shock revisited: Solving the puzzle of blast trauma. Science **319**, 406–408 (2008). doi:10.1126/science.319.5862.406

20. Cernak, I., Merkle, A.C., Koliatsos, V.E., Bilik, J.M., Luong, Q.T., Mahota, T.M., Xu, L., Slack, N., Windle, D., Ahmed, F.A.: The pathobiology of blast injuries and blast-induced neuro-trauma as identified using a new experimental model of injury in mice. Neurobiol. Dis. **41**(2), 538–551 (2011). doi:10.1016/j.nbd.2010.10.025

21. Courtney, A.C., Courtney, M.W.: A thoracic mechanism of mild traumatic brain injury due to blast pressure waves. Med. Hypotheses **72**(1), 76–83 (2009). doi:10.1016/j.mehy.2008.08.015

22. Courtney, M., Courtney, A.: History and evidence regarding hydrostatic shock. Neurosurgery **68**(2), E596–E598 (2011). doi:10.1227/NEU.0b013e3182041992

23. Needham, C.E., Ritzel, D., Rule, G.T., Wiri, S., Young, L.: Blast testing issues and TBI: experimental models that lead to wrong conclusions. Front. Neurol. **6**, 72 (2015). doi:10.3389/fneur.2015.00072

24. Moss, W.C., King, M.J., Blackman, E.G.: Distinguishing realistic military blasts from firecrackers in mitigation studies of blast-induced traumatic brain injury. PNAS **108**(17), 6691–6692 (2011). doi:10.1073/pnas.1101671108

25. Josey, T., Sawyer, T.W., Ritzel, D., Donahue, L.: High fidelity simulation of free-field blast loading: the importance of dynamic pressure. In: Proceedings of the Personal Armour Systems Symposium 2016, Amsterdam, Netherlands (2016)

26. Stemper, B.D., Shah, A.S., Budde, M.D., Olsen, C.M., Glavaski-Joksimovic, A., Kurpad, S.N., McCrea, M., Pintar, F.A.: Behavioral outcomes differ between rotational acceleration and blast mechanisms of mild traumatic brain injury. Front. Neurol. **7**, 31 (2016). doi:10.3389/fneur.2016.00031

27. Sawyer, T.W., Wang, Y., Ritzel, D.V., Josey, T., Villanueva, M., Shei, Y., Nelson, P., Hennes, G., Weiss, T., Vair, C., Fan, C.: High-fidelity simulation of primary blast: direct effects on the head. J. Neurotrauma **33**, 1181–1193 (2016). doi:10.1089/neu.2015.3914

28. Willinger, R., Taleb, L., Kopp, C.M.: Modal and temporal analysis of head mathematical models. J. Neurotrauma **12**(4), 743–754 (1995). doi:10.1089/neu.1995.12.743

29. Viano, D.C.:Biomechanics of head injury—Toward a theory linking head dynamic motion, brain tissue deformation and neural trauma. In: SAE technical paper 881708 (1988). doi:10.4271/881708

30. Hodgson, V.R., Gurdjian, E.S., Thomas, L.M.: The determination of response characteristics of the head with emphasis on mechanical impedance techniques. In: SAE technical paper 670911 (1967). doi:10.4271/670911

31. Stalnaker, R.L., Fogle, J.L., McElhaney, J.H.: Driving point impedance characteristics of the head. J. Biomech. **4**(2), 127–139 (1971). doi:10.1016/0021-9290(71)90023-6

32. Willinger, R., Baumgartner, D.: Human head tolerance limits to specific injury mechanisms. Int. J. Crashworthiness **8**(6), 605–617 (2003). doi:10.1533/ijcr.2003.0264

33. Ouellet, S., Bouamoul, A., Gauvin, R., Binette, J.S., Williams, K.V., Martineau L.: Development of a biofidelic head surrogate for blast-induced traumatic brain injury assessment. In: Proceedings of the Personal Armor System Symposium 2012, Nuremberg, Germany (2012)

34. Ouellet, S., Bir, C., Bouamoul, A.: Direct comparison of the primary blast response of a physical head model with post-mortem human subjects. In: Proceedings of the Personal Armour System Symposium 2014, Cambridge, UK (2014)

35. Ganpule, S.: Mechanics of blast loading on PMHS and surrogate heads in the study of traumatic brain injury using experimental

and computational approaches. Ph.D. Dissertations, University of Lincoln Nebraska (2013)

36. Merkle, A.C., Wing, I.D., Armiger, R.A., Carkhuff, B.G., Roberts, J.C.: Development of a human head physical surrogate model for investigating blast injury. In: Proceedings of ASME International Mechanical Engineering Congress (2009). doi:10.1115/IMECE2009-11807

37. Roberts, J.C., Merkle, A.C., Carkhuff, B.G.,Wing, I.D., Leese, G.B.: Methods and systems to implement a surrogate head model and directly measure brain/skull relative displacement. U.S. Patent 8725449 (2014)

38. Foster, J.K., Kortge, J.O., Wolanin, M.J.: Hybrid III: A biomechanically-based crach test dummy. In: SAE technical paper 770938, (1977). doi:10.4271/770938

39. Bir, C., Bolander, R., Leonardi, A., Ritzel, D., VandeVord, P., Dingell, J.D.: A biomechanical prospective of blast injury neuro-trauma. In: Proceedings of HFM-207 NATO Symposium on Survey of Blast Injury Across the Full Landscape of Military Science, MP-HFM-207-27, Halifax, Canada. doi:10.14339/RTO-MP-HFM-207-27-doc

40. Yoganandan, N., Pintar, F.A., Zhang, J., Baisden, J.L.: Physical properties of the human head: mass, center of gravity and moment of inertia. J. Biomech. **42**(9), 1177–1192 (2009). doi:10.1016/j.jbiomech.2009.03.029

41. Fry, F.J., Barger, J.E.: Acoustical properties of the human skull. J. Acoust. Soc. Am. **63**(5), 1576–1590 (1978). doi:10.1121/1.381852

42. Pichardo, S., Sin, V.W., Hynynen, K.: Multi-frequency characterization of the speed of sound and attenuation coefficient for longitudinal transmission of freshly excised human skulls. Phys. Med. Biol. **56**(1), 219 (2011). doi:10.1088/0031-9155/56/1/014

43. Stenfelta, S., Goode, R.L.: Transmission properties of bone conducted sound: Measurements in cadaver heads. J Acoust. Soc. Am. **118**, 2373–2391 (2005). doi:10.1121/1.2005847

44. Appleby-Thomas, G.J., Hazell, P.J., Sheldon, R.P., Stennett, C., Hameed, A., Wilgeroth, J.M.: The high strain-rate behaviour of selected tissue analogues. J. Mech. Beh. Biomed. Mat **33**, 124–135 (2014). doi:10.1016/j.jmbbm.2013.05.018

45. Brands, D.W., Boveendeerd, P.H., Peters, G.W., Wismans, J.S.: The large strain dynamic behaviour of in-vitro porcine brain tissue and a silicone gel model material. Stapp Car Crash J. **44**, 249–260 (2000)

46. Kremkau, F.W., Barnes, R.W., McGraw, C.P.: Ultrasonic attenuation and propagation speed in normal human brain. J. Acoust. Soc. Am. **70**(1), 29–38 (1981). doi:10.1121/1.386578

47. Glasstone, S., Dolan, P.J.: The effects of nuclear weapons. US Department of Defense, DITC report ADA087568. http://www.dtic.mil/get-tr-doc/pdf?AD=ADA087568 (1977). Accessed 28 Aug 2017